On the generation of nonlinear damage resonance intermodulation for elastic wave spectroscopy

Francesco Ciampa,[1] Gennaro Scarselli,[2] and Michele Meo[1,a)]
[1]*Department of Mechanical Engineering, University of Bath, Bath BA2 7AY, United Kingdom*
[2]*Department of Engineering for Innovation, University of Salento, Lecce 73100, Italy*

(Received 13 May 2016; revised 10 March 2017; accepted 14 March 2017; published online 4 April 2017)

Recent nonlinear elastic wave spectroscopy experiments have shown that the nonlinear ultrasonic response of damaged composite materials can be enhanced by higher vibrations at the local damage resonance. In this paper, the mathematical formulation for the generation of nonlinear wave effects associated with continuous periodic excitation and the concept of local defect resonance is provided. Under the assumption of both quadratic and cubic approximation, the existence of higher harmonics of the excitation frequency, superharmonics of the damage resonance frequency and nonlinear wave effects, here named as nonlinear damage resonance intermodulation, which correspond to the nonlinear intermodulation between the driving and the damage resonance frequencies, is proved. All these nonlinear elastic effects are caused by the interaction of propagating ultrasonic waves with the local damage resonance and can be measured at locations different from the material defect one. The proposed analytical model is confirmed and validated through experimental transducer-based measurements of the steady-state nonlinear resonance response on a damaged composite sample. These results will provide opportunities for early detection and imaging of material flaws. © *2017 Acoustical Society of America*. [http://dx.doi.org/10.1121/1.4979256]

[JFL] Pages: 2364–2374

I. INTRODUCTION

The major difficulty in the characterisation of a material degradation process is due to the fact that the medium, either metallic or multi-layered composite, exhibits very few measurable signs of damage prior to the onset of micro-cracks or delamination, which often precede catastrophic failures. Most of current inspections are performed using conventional linear ultrasonic (LU) non-destructive evaluation (NDE) and structural health monitoring (SHM) techniques, which measure either the reflection and scattering of primary waves at the material heterogeneities and discontinuities (e.g., wave speed, damping variations, etc.) or the impedance contrasts from open interfaces such as holes, voids, and free surfaces.[1] However, these techniques are not able to detect small defects before they grow to a critical size of few millimetres, as the contribution on the total structural stiffness and the elastic scattering from flaws originating at incipient stages of damage development is negligible. Nonlinear elastic wave spectroscopy (NEWS) methods are an alternative to traditional LU techniques for early stage and micro-damage detection, as they explicitly interrogate the material nonlinear elastic behaviour and its effect on the wave propagation caused by the presence of defects. Examples of NEWS methods are higher harmonics features extraction (HH),[2] nonlinear elastic wave modulation (NEWM),[3] scaling subtraction (SSM),[4] and phase symmetry analysis (PSA).[5,6] These techniques have shown an extreme sensitivity in diagnosing manufacturing defects such as porosity, component assembly contact conditions, and incipient damage in the form of micro-cracks, delaminations, clapping areas, and adhesive bond weakening.[7] Indeed, nonlinearities, discontinuities and hysteresis in the microscopic stress-strain relation of tiny cracks may result in a variety of nonlinear ultrasonic phenomena, which become measurable at the macroscopic (structural) level in the form of higher harmonics of the monochromatic input tone, as well as modulation of multiple excitation frequencies.[8] Such harmonics can be attributed either to the "clapping/rubbing" motion of the region normal to the damage interface or to the nonlinear friction between the defect surfaces, which are excited by small tangential stresses produced by the elastic waves propagating through the medium.[9,10] In terms of strain amplitude, second order harmonic is principally used a signature for damage characterisation of materials that manifest "classical" or "anharmonic" nonlinear behaviour at the atomic/molecular scale (i.e., in the sense of Landau[11]). In addition to "classical" nonlinear elastic effects, a new family of nonlinear material features known as "non-classical" was experimentally observed for structural flaws,[12,13] including the nonlinear local defect resonance (LDR) effect.[14] This last elastic phenomenon has gained considerable attention in the past few years as it allows selective ultrasonic activation and higher sensitivity to the presence of structural flaws. LDR shall be referred as the interaction of acoustic/ultrasonic waves with the damaged area at a frequency matching the defect resonance, which results in a substantial enhancement of the vibration amplitude only in the localised damaged region. Indeed, using wide-band excitation, LDR exhibits transitions from linear to nonlinear regime with the effect of generating higher and sub-harmonics of the input frequency. Although recent studies have demonstrated the capabilities of fully non-contact linear and nonlinear LDR to detect dynamic

a)Electronic mail: m.meo@bath.ac.uk

 0001-4966/2017/141(4)/2364/11/$30.00

frequency shifts in nonlinear resonant ultrasonic spectroscopy (NRUS),[15] near-surface and in-depth delamination in digital shearography,[16] and laser vibrometry imaging,[17] its use in fully contact applications with continuous periodic excitation is still limited. Indeed, using tone burst excitation, the nonlinear LDR response is enhanced by higher vibration amplitudes measured only at its local resonance and zero elsewhere. This implies that these material nonlinear effects can be sensed exclusively at the defect location.

In this paper, we provide a two-dimensional (2D) mathematical description and an experimental validation of the generation of both "classical" and "non-classical" nonlinear elastic effects associated with fully contact nonlinear LDR and harmonic input measured at all points of the medium's surface. Beside higher harmonics and superharmonics, novel nonlinear elastic wave phenomena, here named as *nonlinear damage resonance intermodulation* (NDRI), which corresponds to a nonlinear intermodulation between the driving frequency, f_0, and the frequency of the LDR, f_d, were found. A perturbation theory applied to the equation of motion governing bending deflection was used to describe the nonlinear structural response on a damaged composite plate. Transducer-based contact tests were carried out on a composite laminate with controlled delamination. Both analytical and experimental results showed the generation of nonlinear elastic effects, including NDRI, related to the interaction of the flexural waves with the steady-state nonlinear LDR response.

II. THEORETICAL MODEL OF NONLINEAR LDR

When the frequency f_0 of the driving flexural wave is matched to the LDR frequency, f_d, of the damaged composite plate of thickness h, the vibration amplitude of the portion of volume with depth d below the defect dramatically increases (Fig. 1). This is due to a local decrease in stiffness for a certain structural mass in the damaged region, which manifests in a particular characteristic frequency f_d.

Assuming that the internal structural flaw such as delamination in a composite laminate is represented by a flat bottom hole (FBH), i.e., a thin circular defect of radius r and thickness s, the expression of the LDR frequency becomes[18]

$$f_d \cong \frac{1.6d}{r^2}\sqrt{\frac{E}{12\rho(1-\upsilon^2)}}, \tag{1}$$

where E and υ are the effective elastic modulus and Poisson's ratio of the composite laminate, respectively, and ρ is the density. Equation (1) corresponds to the first bending mode of a circular plate with clamped boundaries and can be also used to evaluate LDR in other structural flaws and materials such as laminar defects in rolled sheets metals.[17]

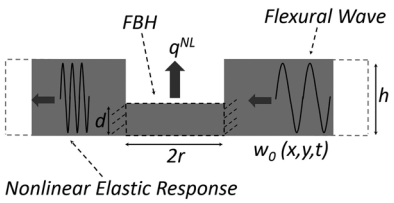

FIG. 1. Illustration of the nonlinear LDR effect for the case of a flat bottom hole (FBH) using the quadratic and cubic approximation of the nonlinear force q^{NL} associated to the bending displacement $w_0(x,y,t)$. In this figure, h is the thickness of the damaged composite plate, d is the depth of the portion of volume below the defect of radius r.

Since the local resonance vibration of cracks enhances the generation of nonlinear material phenomena, an efficient energy pumping of nonlinear ultrasonic waves can be achieved, thus leading to higher sensitivity to the presence of the damage. Solodov[19] proposed a 1D model based on a nonlinear damped oscillator in order to describe the generation of higher harmonics (superharmonics) and subharmonics effects of the LDR frequency. However, this model assumed that these material nonlinear effects could be sensed exclusively at the LDR location.

This research confirms the results obtained by Solodov, and provides a 2D mathematical model for the generation of nonlinear elastic effects associated to the LDR, which can be features not only at the damage location, but at all points of the medium's surface simply using harmonic excitation. In other words, this paper demonstrates that the nonlinear LDR is not just a local effect, and the interaction of propagating waves with the LDR generates nonlinear elastic wave phenomena, including the newly found NDRI, which can also be sensed at locations different from the damage resonance.

In the proposed theoretical model, a quadratic and cubic nonlinear approximation of the force q^{NL} associated to the out-of-plane (bending) displacement w_0 in classical laminate plate theory is used to describe the nonlinear elastic effects of LDR. Assuming a thickness-to-width ratio smaller than 0.1 (i.e., neglecting the rotator inertia) and zero in-plane and thermal forces, the nonlinear equation of motion governing bending deflection for a symmetric composite plate is

$$\begin{aligned} &D_{11}\frac{\partial^4 w_0(x,y,t)}{\partial x^4} + 2(D_{12}+2D_{66})\frac{\partial^4 w_0(x,y,t)}{\partial x^2 \partial y^2} \\ &+ D_{22}\frac{\partial^4 w_0(x,y,t)}{\partial y^4} + I_0\frac{\partial^2 w_0(x,y,t)}{\partial t^2} \\ &- q(x,y,t) + q^{\mathrm{NL}}(\xi,\eta,x,y,t) = 0. \end{aligned} \tag{2}$$

In Eq. (2), $q(x,y,t)$ is the applied sinusoidal transverse force, $q^{\mathrm{NL}}(\xi,\eta,x,y,t)$ is the nonlinear force containing the quadratic and cubic terms associated with the nonlinear LDR, $q^{II}(\xi,x,y,t)$, and $q^{III}(\eta,x,y,t)$, respectively, with ξ and η the second and third order nonlinear coefficients (constants), and D_{11}, D_{12}, and D_{66} are the component of the bending stiffness matrix D_{ij} defined in terms of the plane stress-reduced stiffnesses for the kth orthotropic lamina $\bar{Q}_{ij}^{(k)}$.[20] This is expressed as follows:

$$D_{ij} = \frac{1}{3}\sum_{k=1}^{L}\bar{Q}_{ij}^{(k)}\left(z_{k+1}^3 - z_k^3\right). \tag{3}$$

The kth layer in Eq. (3) is located between the points $z = z_k$ and $z = z_{k+1}$ in the thickness direction. Finally, I_0 in Eq. (2) is the mass moment defined as

$$I_0 = \sum_{k=1}^{L}\rho^{(k)}(z_{k+1} - z_k). \tag{4}$$

Equation (2) is a nonlinear, non-homogeneous ordinary differential equations (ODE) associated with the following boundary conditions for a simply supported plate:

$$w_0(x,0,t)=0,\quad w_0(x,b,t)=0,\quad w_0(0,y,t)=0,\quad w_0(a,y,t)=0 \text{ for } t\geq 0, \tag{5a}$$

$$M_{xx}(0,y,t)=0,\quad M_{xx}(a,y,t)=0,\quad M_{yy}(x,0,t)=0,\quad M_{yy}(x,b,t)=0 \text{ for } t\geq 0, \tag{5b}$$

with a and b are the length and width of the plate along the x- and y-axis, respectively, and M_{xx}, M_{yy}, and M_{zz} the moments in the x, y, and z coordinates. The initial conditions associated with Eq. (2) at $t=0$ are $w_0(x,y,0)=0$ and $\partial w_0(x,y,0)/\partial t=0$ for all x and y. Assuming that the second and third order nonlinear responses originated from the nonlinear term $q^{II}(\xi,x,y,t)$ and $q^{III}(\eta,x,y,t)$ are much smaller than the fundamental one, a first order perturbation theory can be used to solve Eq. (2):

$$w_0(x,y,t)=w_0^{(1)}(x,y,t)+\xi w_0^{(2)}(x,y,t)+\eta w_0^{(3)}(x,y,t)+O(\xi^2,\eta^2). \tag{6}$$

Substituting Eq. (6) into Eq. (2) and neglecting the quadratic terms $O(\xi^2,\eta^2)$, the following equation can be obtained:

$$\begin{aligned}&D_{11}\frac{\partial^4\left[w_0^{(1)}(x,y,t)+\xi w_0^{(2)}(x,y,t)+\eta w_0^{(3)}(x,y,t)\right]}{\partial x^4}+2(D_{12}+2D_{66})\frac{\partial^4\left[w_0^{(1)}(x,y,t)+\xi w_0^{(2)}(x,y,t)+\eta w_0^{(3)}(x,y,t)\right]}{\partial x^2\partial y^2}\\&+D_{22}\frac{\partial^4\left[w_0^{(1)}(x,y,t)+\xi w_0^{(2)}(x,y,t)+\eta w_0^{(3)}(x,y,t)\right]}{\partial y^4}+I_0\frac{\partial^2\left[w_0^{(1)}(x,y,t)+\xi w_0^{(2)}(x,y,t)+\eta w_0^{(3)}(x,y,t)\right]}{\partial t^2}\\&-q(x,y,t)+q^{II}(\xi,x,y,t)+q^{III}(\eta,x,y,t)=0.\end{aligned} \tag{7}$$

A. Linear solution

The solution of the linear inhomogeneous problem associated with Eq. (2) is obtained by posing $q^{II}(\xi,x,y,t)=q^{III}(\eta,x,y,t)=0$. The determination of the linear solution $w_0^{(1)}(x,y,t)$, for all times $t\geq 0$ under any applied load $q(x,y,t)$, is obtained through an expansion of the transverse deflection that satisfies the boundary conditions (5) as follows:

$$w_0^{(1)}(x,y,t)=\sum_{n=1}^{\infty}\sum_{m=1}^{\infty}W_{mn}(t)\sin(\alpha x)\sin(\beta y), \tag{8}$$

where $\alpha=m\pi/a$, $\beta=n\pi/b$, and $W_{mn}(t)$ are coefficients to be determined such that the governing Eq. (2) is satisfied everywhere in the domain of the plate for $m,n=1,2,3,\ldots$. The transverse load, initial displacement and initial velocity can also be expanded in the series form as

$$q(x,y,t)=\sum_{n=1}^{\infty}\sum_{m=1}^{\infty}Q_{mn}(t)\sin(\alpha x)\sin(\beta y), \tag{9}$$

$$d_0(x,y,t)=\sum_{n=1}^{\infty}\sum_{m=1}^{\infty}D_{mn}(t)\sin(\alpha x)\sin(\beta y), \tag{10}$$

$$v_0(x,y,t)=\sum_{n=1}^{\infty}\sum_{m=1}^{\infty}V_{mn}(t)\sin(\alpha x)\sin(\beta y), \tag{11}$$

where for a point source harmonic load $f(t)=\cos(2\pi f_0 t)$ of amplitude Q_0 located at (x_0,y_0), the load coefficients $Q_{mn}(t)$ are given by

$$\begin{aligned}Q_{mn}(t)&=\frac{4}{ab}\cos(\omega_0 t)\int_0^b\int_0^a Q_0\delta(x-x_0,y-y_0)\\&\quad\times\sin(\alpha x)\sin(\beta y)dx\,dy\\&=\frac{4Q_0}{ab}\sin(\alpha x_0)\sin(\beta y_0)\cos(2\pi f_0 t).\end{aligned} \tag{12}$$

Substitution of Eqs. (8), (9), and (12) into Eq. (7) leads to

$$K_{mn}W_{mn}(t)+I_0\frac{\partial^2 W_{mn}(t)}{\partial t^2}=Q_{mn}(t), \tag{13}$$

where $K_{mn}=[D_{11}\alpha^4+2(D_{12}+2D_{66})\alpha^2\beta^2+D_{22}\beta^4]$. Equation (13) is valid for every point $(x,\ y)$ of the domain $0<x<a$ and $0<y<b$ and can be rewritten as

$$\frac{\partial^2 W_{mn}(t)}{\partial t^2}+\left(\frac{K_{mn}}{I_0}\right)W_{mn}(t)=\bar{Q}_{mn}(t), \tag{14}$$

with $\bar{Q}_{mn}(t)=Q_{mn}(t)/I_0$. The solution of the above equation is given by

$$\begin{aligned}W_{mn}(t)&=C_1u_1(t)+C_2u_2(t)+W_{mn}^p(t)\\&=C_1e^{\lambda_1 t}+C_2e^{\lambda_2 t}+W_{mn}^p(t),\end{aligned} \tag{15}$$

where C_1 an C_2 are constants to be determined using the initial conditions and $W_{mn}^p(t)$ is the particular solution given by[20]

$$W^{p}_{mn}(t) = \int_t \frac{u_1(\tau)u_2(t) - u_1(t)u_2(\tau)}{u_1(\tau)\dot{u}_2(\tau) - \dot{u}_1(\tau)u_2(\tau)} \bar{Q}_{mn}(\tau)d\tau, \tag{16}$$

where $\lambda_1 = -i2\pi f_{mn}$ and $\lambda_2 = i2\pi f_{mn}$ are the roots of equation $\lambda_i^2 + (2\pi f_{mn})^2 = 0$ and $f_{mn} = \sqrt{K_{mn}/I_0}/2\pi$ is the natural frequency of the fully supported composite laminate. The general solution of the linear non-homogeneous ODE (14) is

$$W_{mn}(t) = C_1 \cos(2\pi f_{mn}t) + C_2 \sin(2\pi f_{mn}t) + \frac{\bar{Q}_{mn}}{4\pi^2\left(f_{mn}^2 - f_0^2\right)} \cos(2\pi f_0 t). \tag{17}$$

The particular solution of Eq. (17) corresponds to the steady-state oscillation of the exciting force at frequency f_0. Assuming that the displacement and velocity in Eqs. (10) and (11) are equal to zero at $t = 0$, the linear bending deflection becomes

$$w_0^{(1)}(x,y,t) = \sum_{n=1}^{\infty}\sum_{m=1}^{\infty} A^I[\cos(2\pi f_0 t) - \cos(2\pi f_{mn}t)] \times \sin(\alpha x)\sin(\beta y) \tag{18}$$

with $A^I = \bar{Q}_{mn}/[4\pi^2(f_{mn}^2 - f_0^2)]$. If f_d is the frequency associated with the LDR located at coordinates $x = x_d$ and $y = y_d$ [analytically obtained using Eq. (1)], it can be seen from Eq. (18) that the maximum linear amplitude vibration is obtained when $f_{mn} = f_d = f_0$, i.e., when the driving frequency matches the LDR frequency. Equation (18) confirms the results obtained by Solodov[19] using wide-band excitation and opens new scenarios for novel nonlinear elastic effects that will be analysed in Secs. II B and II C.

B. Quadratic nonlinear approximation

The second order nonlinear elastic effect generated at the LDR location (x_d, y_d) is here considered by defining the second order nonlinear transverse load $F^{II}_{mn}(\xi,t)$ through the *quadratic nonlinear approximation* as follows:

$$F^{II}_{mn}(\xi,t) = \xi\left[\frac{\bar{Q}_{mn}}{4\pi^2\left(f_d^2 - f_0^2\right)}[\cos(2\pi f_0 t) - \cos(2\pi f_d t)]\sin(\alpha x_d)\sin(\beta y_d)\right]^2 = \xi A^{II}[\cos(2\pi f_0 t) - \cos(2\pi f_d t)]^2, \tag{19}$$

where $A^{II} = [\bar{Q}_{mn}/[4\pi^2(f_d^2 - f_0^2)]\sin(\alpha x_d)\sin(\beta y_d)]^2$. The second order nonlinear transverse load in Eq. (2) can be rewritten as

$$q^{II}(\xi,x,y,t) = \sum_{m=1}^{\infty}\sum_{n=1}^{\infty} F^{II}_{mn}(\xi,t)\sin(\alpha x)\sin(\beta y), \tag{20}$$

and assuming an expansion of the transverse deflection satisfying the homogeneous boundary conditions of the simply supported plate, we obtain

$$w_0^{(2)}(x,y,t) = \sum_{n=1}^{\infty}\sum_{m=1}^{\infty} Y_{mn}(t)\sin\alpha x \sin\beta y. \tag{21}$$

Substituting Eqs. (20) and (21) into Eq. (7) yields

$$\xi Y_{mn}\left[D_{11}\alpha^4 + 2(D_{12} + 2D_{66})\alpha^2\beta^2 + D_{22}\beta^4\right] + \xi I_0 \ddot{Y}_{mn} = -F^{II}_{mn}, \tag{22}$$

which becomes

$$4\pi^2 Y_{mn} f_{mn}^2 + \ddot{Y}_{mn} = -\bar{A}^{II}[\cos(2\pi f_0 t) - \cos(2\pi f_d t)]^2, \tag{23}$$

with $\bar{A}^{II} = A^{II}/I_0$.

The general solution of Eq. (22) is

$$Y_{mn}(t) = C_1 y_1 + C_2 y_2 + Y^p_{mn}(t) = C_1 e^{-i2\pi f_{mn}t} + C_2 e^{i2\pi f_{mn}t} + Y^p_{mn}(t), \tag{24}$$

where $y_1 = e^{-i2\pi f_{mn}t}$ and $y_2 = e^{i2\pi f_{mn}t}$ are the solution for the homogeneous counterpart. The particular solution $Y^p_{mn}(t)$ can be found using the method of variation of parameters for non-homogeneous linear ODEs, which is, for the sake of clarity, reported in the Appendix. The solution of Eq. (23) is obtained by substituting Eq. (A8) into Eq. (21):

$$w_0^{(2)}(x,y,t) = \sum_{n=1}^{\infty}\sum_{m=1}^{\infty}\left\{\bar{A}^{II}\left[\frac{1 - \cos(2\pi f_{mn}t)}{4\pi^2 f_{mn}^2} + \frac{\cos(2\pi f_{mn}t) - \cos(4\pi f_0 t)}{4\pi^2\left(4f_0^2 - f_{mn}^2\right)} + \frac{\cos(2\pi f_{mn}t) - \cos(4\pi f_d t)}{4\pi^2\left(4f_d^2 - f_{mn}^2\right)} + \frac{\cos[2\pi(f_0 \pm f_d)t] - \cos(2\pi f_{mn}t)}{\left[(2\pi f_0 \pm 2\pi f_d)^2 - 4\pi^2 f_{mn}^2\right]}\right]\right\}\sin\alpha x \sin\beta y. \tag{25}$$

C. Cubic nonlinear approximation

The third order nonlinear elastic effect generated at the LDR location (x_d, y_d) is obtained by defining the third order nonlinear transverse load $F^{III}_{mn}(\eta, t)$ through the following *cubic nonlinear approximation*:

$$F^{III}_{mn}(\eta,t) = \eta\left[\frac{\bar{Q}_{mn}}{4\pi^2\left(f_d^2 - f_0^2\right)}\sin(\alpha x_d)\sin(\beta y_d)[\cos(2\pi f_0 t) - \cos(2\pi f_d t)]\right]^3$$
$$= \eta A^{III}[\cos(2\pi f_0 t) - \cos(2\pi f_d t)]^3, \tag{26}$$

where $A^{III} = [\bar{Q}_{mn}/[4\pi^2(f_d^2 - f_0^2)]\sin(\alpha x_d)\sin(\beta y_d)]^3$. The third order nonlinear transverse load in Eq. (2) can be rewritten as

$$q^{III}(\xi, x, y, t) = \sum_{m=1}^{\infty}\sum_{n=1}^{\infty} F^{III}_{mn}(\xi, t)\sin(\alpha x)\sin(\beta y). \tag{27}$$

Similarly to the second order nonlinear case, assuming an expansion of the transverse deflection satisfying the homogeneous boundary conditions of the simply supported plate, yields

$$w_0^{(3)}(x, y, t) = \sum_{n=1}^{\infty}\sum_{m=1}^{\infty} \Psi_{mn}(t)\sin(\alpha x)\sin(\beta y). \tag{28}$$

Substituting Eqs. (27) and (28) into Eq. (2) yields

$$\eta\Psi_{mn}\left[D_{11}\alpha^4 + 2(D_{12} + 2D_{66})\alpha^2\beta^2 + D_{22}\beta^4\right] + \eta I_0\ddot{\Psi}_{mn} = -F^{III} \tag{29}$$

or

$$4\pi^2\Psi_{mn}f_{mn}^2 + \ddot{\Psi}_{mn} = -\bar{A}^{III}[\cos(2\pi f_0 t) - \cos(2\pi f_d t)]^3, \tag{30}$$

with $\bar{A}^{III} = A^{III}/I_0$. Again, since the displacement and velocity are equal to zero for $t = 0$, the total solution of Eq. (30) becomes

$$\Psi_{mn}(t) = \frac{\bar{A}^{III}}{4}\left[\frac{9[\cos(2\pi f_{mn}t) - \cos(2\pi f_0 t)]}{4\pi^2\left(f_0^2 - f_{mn}^2\right)} + \frac{\cos(2\pi f_{mn}t) - \cos(6\pi f_0 t)}{4\pi^2\left(9f_0^2 - f_{mn}^2\right)} + \frac{9[\cos(2\pi f_d t) - \cos(2\pi f_{mn}t)]}{4\pi^2\left(f_d{}^2 - f_{mn}^2\right)}\right.$$
$$+ \frac{\cos(6\pi f_d t) - \cos(2\pi f_{mn}t)}{4\pi^2\left(9f_d{}^2 - f_{mn}^2\right)} + \frac{3[\cos[2\pi(2f_0 \pm f_d)t] - \cos(2\pi f_{mn}t)]}{\left[(4\pi f_0 \pm 2\pi f_d)^2 - 4\pi^2 f_{mn}^2\right]}$$
$$\left. + \frac{3[\cos(2\pi f_{mn}t) - \cos[2\pi(f_0 \pm 2f_d)t]]}{\left[(2\pi f_0 \pm 4\pi f_d)^2 - 4\pi^2 f_{mn}^2\right]}\right]. \tag{31}$$

Substituting Eq. (31) into Eq. (28), yields

$$w_0^{(3)}(x, y, t) = \sum_{n=1}^{\infty}\sum_{m=1}^{\infty}\left\{\frac{\bar{A}^{III}}{4}\left[\frac{9[\cos(2\pi f_{mn}t) - \cos(2\pi f_0 t)]}{4\pi^2\left(f_0^2 - f_{mn}^2\right)} + \frac{\cos(2\pi f_{mn}t) - \cos(6\pi f_0 t)}{4\pi^2\left(9f_0^2 - f_{mn}^2\right)}\right.\right.$$
$$+ \frac{9[\cos(2\pi f_d t) - \cos(2\pi f_{mn}t)]}{4\pi^2\left(f_d{}^2 - f_{mn}^2\right)} + \frac{\cos(6\pi f_d t) - \cos(2\pi f_{mn}t)}{4\pi^2\left(9f_d{}^2 - f_{mn}^2\right)}$$
$$+ \frac{3[\cos[2\pi(2f_0 \pm f_d)t] - \cos(2\pi f_{mn}t)]}{\left[(4\pi f_0 \pm 2\pi f_d)^2 - 4\pi^2 f_{mn}^2\right]}$$
$$\left.\left. + \frac{3[\cos(2\pi f_{mn}t) - \cos[2\pi(f_0 \pm 2f_d)t]]}{[(2\pi f_0 \pm 4\pi f_d)^2 - 4\pi^2 f_{mn}^2]}\right]\right\}\sin\alpha x \sin\beta y. \tag{32}$$

Substituting Eqs. (18), (25), and (32) into Eq. (6), the total solution of the differential problem (2) is

$$w_0(x,y,t) = w_0^{(1)}(x,y,t) + \xi w_0^{(2)}(x,y,t) + \eta w_0^{(3)}(x,y,t)$$
$$= \sum_{n=1}^{\infty}\sum_{m=1}^{\infty} A^{I}[\cos(2\pi f_0 t) - \cos(2\pi f_{mn} t)]\sin(\alpha x)\sin(\beta y)$$
$$+\xi\sum_{n=1}^{\infty}\sum_{m=1}^{\infty}\left[\frac{\bar{A}^{II}}{2}(S_1 + S_2 + S_3 + S_4 + S_5)\right]\sin(\alpha x)\sin(\beta y)$$
$$+\eta\sum_{n=1}^{\infty}\sum_{m=1}^{\infty}\left[\frac{\bar{A}^{III}}{4}(T_1 + T_2 + T_3 + T_4 + T_5 + T_6 + T_7 + T_8)\right]\sin(\alpha x)\sin(\beta y), \quad (33)$$

with,

$$S_1 = \frac{[1-\cos(2\pi f_{mn} t)]}{4\pi^2 f_{mn}^2}, \quad S_2 = \frac{\cos(2\pi f_{mn} t) - \cos(4\pi f_0 t)}{4\pi^2\left(4f_0^2 - f_{mn}^2\right)}, \quad S_3 = \frac{\cos(2\pi f_{mn} t) - \cos(4\pi f_d t)}{4\pi^2\left(4f_d^2 - f_{mn}^2\right)},$$
$$S_{4,5} = \frac{2\{\cos[2\pi(f_0 \pm f_d)t] - \cos(2\pi f_{mn} t)\}}{\left[(2\pi f_0 \pm 2\pi f_d)^2 - 4\pi^2 f_{mn}^2\right]}, \quad T_1 = \frac{9[\cos(2\pi f_{mn} t) - \cos(2\pi f_0 t)]}{4\pi^2\left(f_0^2 - f_{mn}^2\right)}, \quad T_2 = \frac{\cos(2\pi f_{mn} t) - \cos(6\pi f_0 t)}{4\pi^2\left(9f_0^2 - f_{mn}^2\right)},$$
$$T_3 = \frac{9[\cos(2\pi f_d t) - \cos(2\pi f_{mn} t)]}{4\pi^2\left(f_d{}^2 - f_{mn}^2\right)}, \quad T_4 = \frac{\cos(6\pi f_d t) - \cos(2\pi f_{mn} t)}{4\pi^2\left(9f_d{}^2 - f_{mn}^2\right)}, \quad T_{5,6} = \frac{3\{\cos[2\pi(2f_0 \pm f_d)t] - \cos(2\pi f_{mn} t)\}}{\left[(4\pi f_0 \pm 2\pi f_d)^2 - 4\pi^2 f_{mn}^2\right]} \quad \text{and}$$
$$T_{7,8} = \frac{3\{\cos(2\pi f_{mn} t) - \cos[2\pi(f_0 \pm 2f_d)t]\}}{\left[(2\pi f_0 \pm 4\pi f_d)^2 - 4\pi^2 f_{mn}^2\right]}.$$

From the results of Eq. (33), the generation of "classical" nonlinear and "non-classical" nonlinear LDR effects falls into two main conditions. In the first condition, material nonlinear phenomena can occur if the amplitude terms A^{II} and A^{III} in Eq. (33) tend to infinity, i.e., when the excitation frequency, f_0, is equal of the LDR frequency, f_d. Under this condition, Eq. (33) features a number of nonlinear elastic phenomena for the resonant defect. Beside the dc terms S_1, T_1 and T_3, "classical" nonlinear second and third harmonic terms of the fundamental frequency S_2 and T_2 and the "non-classical" nonlinear second and third superharmonic terms of the LDR frequency S_3 and T_4 can be generated. Moreover, further "non-classical" nonlinear elastic features obtained as a combination of frequencies f_0 and f_d, here named as NDRI (expressed by the terms S_4, S_5, T_5, T_6, T_7, and T_8), can also occur. These NDRI effects are different from "classical" nonlinear modulation frequencies, as they are not generated by the use of a dual harmonic excitation and occur only under specific combinations of frequencies f_0, f_d, and the resonance modes f_{mn} of the plate. All these spectral responses can open to novel scenarios of nonlinear resonance phenomena for the damage characterisation.

The second condition is that nonlinear LDR effects are not limited to the case when $f_0 = f_d$, but they can also be generated when the denominator of each term S_n and T_n in Eq. (33) is zero, i.e., when specific combinations of frequencies f_0, f_d, and the resonance modes of the plate f_{mn} are met. This further condition broadens the occurrence of these nonlinear LDR phenomena to other driving frequencies, which can be summarised in Table I.

As an example from Table I, Fig. 2 shows that for the S_3 term the highest nonlinear resonance effect is achieved when one of the resonance modes at the damage location is double of the LDR frequency, i.e., when $f_{mn} = 2f_d$. It should be noted that the use of nonlinear anharmonic resonator to describe non-classical nonlinear material phenomena is not new. As an example, the 1D analytical model of classical nonlinear anharmonic oscillator from Landau[11] is able to describe non-classical effects such as the asymmetrical variations of oscillation amplitudes (also known as "fold-over effect").

III. EXPERIMENTAL SETUP

The nonlinear elastic effects associated to LDR were first analytically studied on a composite carbon fibre reinforced plastic (CFRP) plate with dimensions $180 \times 180 \times 1.6$ mm and stacking sequence of $[0/90/45/-45/90/0]_s$ (Fig. 3). The elastic moduli of the lamina are $E_{11} \approx 136$ GPa, $E_{22} \approx 18.5$ GPa, and $G_{12} \approx 5.8$ GPa, whilst the Poisson's ratio is $\nu_{12} \approx 0.29$ and the density is $\rho \approx 1546$ kg/m^3. The location of

TABLE I. Summary of the generation of nonlinear LDR effects for each term in Eq. (33) as a function of the frequencies f_0, f_d, and f_{mn}.

Nonlinear Terms	Nonlinear effects	Conditions on driving frequency
S_2	*Second harmonic* $4\pi f_0$	$f_0 = f_{mn}/2$
S_3	*Superharmonic* $4\pi f_d$	$f_d = f_{mn}/2$
S_4	*NDRI* $2\pi(f_0 + f_d)$	$f_0 = f_{mn} - f_d \Rightarrow (f_{mn} > f_d)$
S_5	*NDRI* $2\pi(f_0 - f_d)$	$f_0 = f_d - f_{mn} \Rightarrow (f_{mn} < f_d)$
T_2	*Third harmonic* $6\pi f_0$	$f_0 = f_{mn}/3$
T_4	*Superharmonic* $6\pi f_d$	$f_d = f_{mn}/3$
T_5	*NDRI* $2\pi(2f_0 + f_d)$	$f_0 = \frac{1}{2}(f_{mn} - f_d) \Rightarrow (f_{mn} > f_d)$
T_6	*NDRI* $2\pi(2f_0 - f_d)$	$f_0 = \frac{1}{2}(f_d - f_{mn}) \Rightarrow (f_{mn} < f_d)$
T_7	*NDRI* $2\pi(f_0 + 2f_d)$	$f_0 = f_{mn} - 2f_d \Rightarrow (f_{mn} > 2f_d)$
T_8	*NDRI* $2\pi(f_0 - 2f_d)$	$f_0 = f_d - 2f_{mn} \Rightarrow (f_{mn} < 2f_d)$

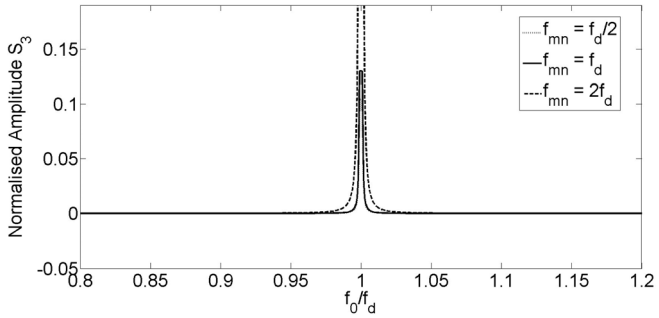

FIG. 2. Analytical result of the normalised amplitude of the S3 term in Eq. (33). The highest nonlinear resonance effect is achieved when one of the resonance modes at the damage location is double of the LDR frequency, i.e., when $f_{mn} = 2f_d$ (dashed line).

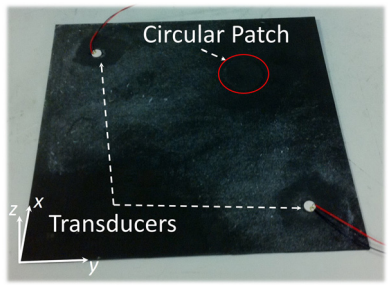

FIG. 3. (Color online) Composite test sample and piezoelectric transducers used during the experimental tests.

the damage was at coordinate $x_d = 125$ mm and $y_d = 60$ mm with the origin at the bottom left corner of the plate. The most well-known technique to introduce artificial in-plane delamination in composites is the inclusion of Teflon inserts in between the laminate plies with different shapes, dimensions, and thickness.[21,22] By assuming a 24 mm in diameter Teflon (double layer) patch located below the fourth layer from the top surface, the LDR frequency was obtained at 11.2 kHz. Such a frequency value was also revealed experimentally as the maximum amplitude response over a sweep signal from 1 to 100 kHz. In order to transmit the input source and measure the material nonlinear response, two surface bonded broadband APC transducers with diameter of 6.35 mm and thickness of 2.55 mm were used both as transmitter and receiver. The transmitter transducer was located at coordinates $x_0 = 30$ mm and $y_0 = 30$ mm and it was linked to a signal amplifier and connected to an arbitrarily waveform generator (TTi-TGA12104) in order to generate continuous sinusoidal waveforms at four different fundamental frequencies, i.e., $f_0 = f_d/3$ (3.733 kHz), $f_0 = f_d/2$ (5.6 kHz), $f_0 = f_d$, and $f_0 = 2f_d$ (22.4 kHz). These excitation values were selected to provide a direct proof of the higher harmonic, superharmonic resonances and NDRI effects as in accordance with Sec. II. The receiver transducer was placed at coordinates $x_r = 150$ mm and $y_r = 150$ mm and it was instrumented with an oscilloscope (Picoscope 4224) with a sampling rate of

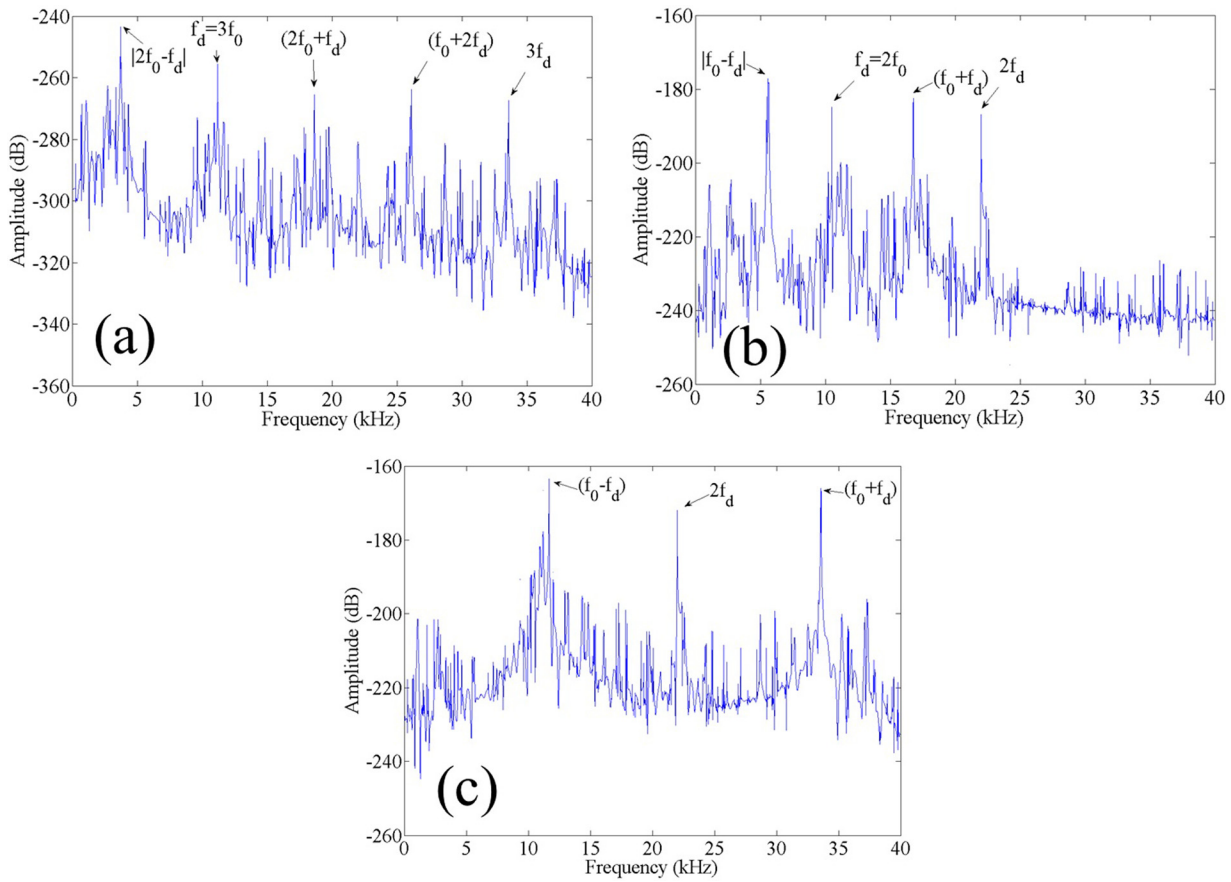

FIG. 4. (Color online) (a)–(c) Analytical spectral result of nonlinear LDR effects obtained at different fundamental frequencies, i.e., 3.733 kHz (a), 5.6 kHz (b), and 22.4 kHz (c) using the S_n and T_n terms in Eq. (33). Each spectrum is measured at location (x_r, y_r) with the damage located at (x_d, y_d) and the transmitter at (x_t, y_t).

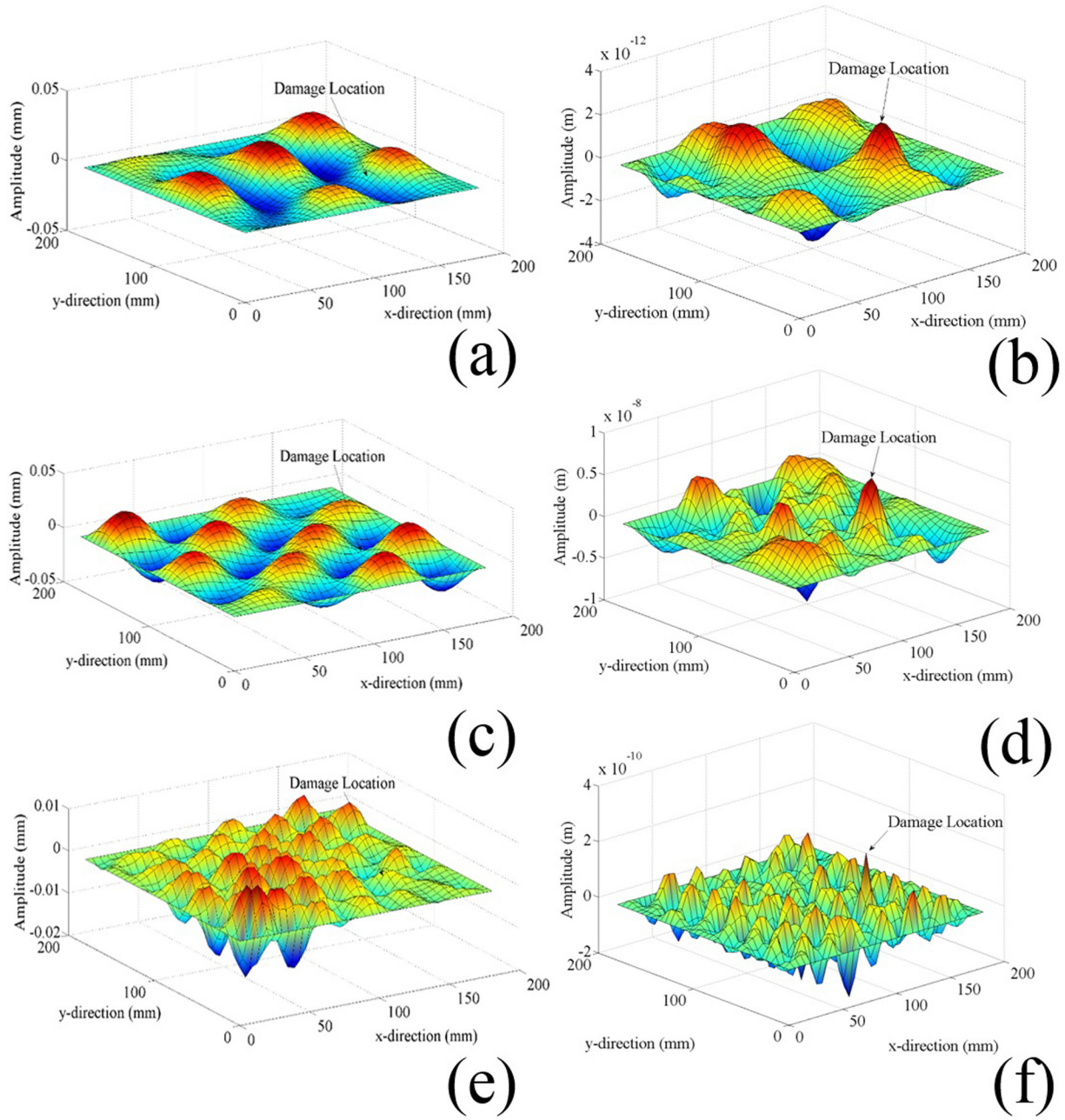

FIG. 5. (Color online) (a)–(f) Analytical linear and nonlinear LDR vibration patterns for 3.733 kHz (a) and (b), 5.6 kHz (c) and (d), and 22.4 kHz (e) and (f).

100 kHz and an acquisition window of $\tau = 200$ ms. The time histories were averaged 20 times in order to improve the signal-to-noise ratio of the measured signals. Additionally, the tested specimen was positioned along the edges on four foam pieces in order to reduce the environmental noise and to simulate fully supported boundary conditions.

IV. ANALYTICAL RESULTS OF NONLINEAR LDR

The analytical results of the nonlinear LDR terms contained in the structural response from Eq. (33) are reported in Fig. 4 for three fundamental frequencies, i.e., $f_0 = f_d/3$, $f_0 = f_d/2$, and $f_0 = 2f_d$. These excitation values were selected to provide a direct proof of the generation of higher harmonics, superharmonic resonances, and NDRI effects in accordance with the results of Sec. II. Only the nonlinear response associated to $f_0 = f_d$ could not be analysed as it represents the particular case in which both nonlinear second and third order out-of-plane displacements tend to infinity. In all the analytical calculations, the same values of the input amplitude $Q_0 = 1 \times 10^4$ Pa and $\xi = \eta = 10$ were used. Figure 4(a) illustrates the nonlinear LDR bending deflection obtained from the nonlinear cubic approximation of the nonlinear second order transverse load for a harmonic frequency equal to one third of the LDR response (3.733 kHz). The frequency spectrum reveals the presence of the nonlinear "classical" third order harmonic term $3f_0$, the superharmonic term $3f_d$ and the NDRI responses $(2f_0 + f_d)$, $(f_0 + 2f_d)$, and $|2f_0 - f_d|$ at the location far away from the damaged area at coordinates $x_r = 150$ mm and $y_r = 150$ mm. By increasing the

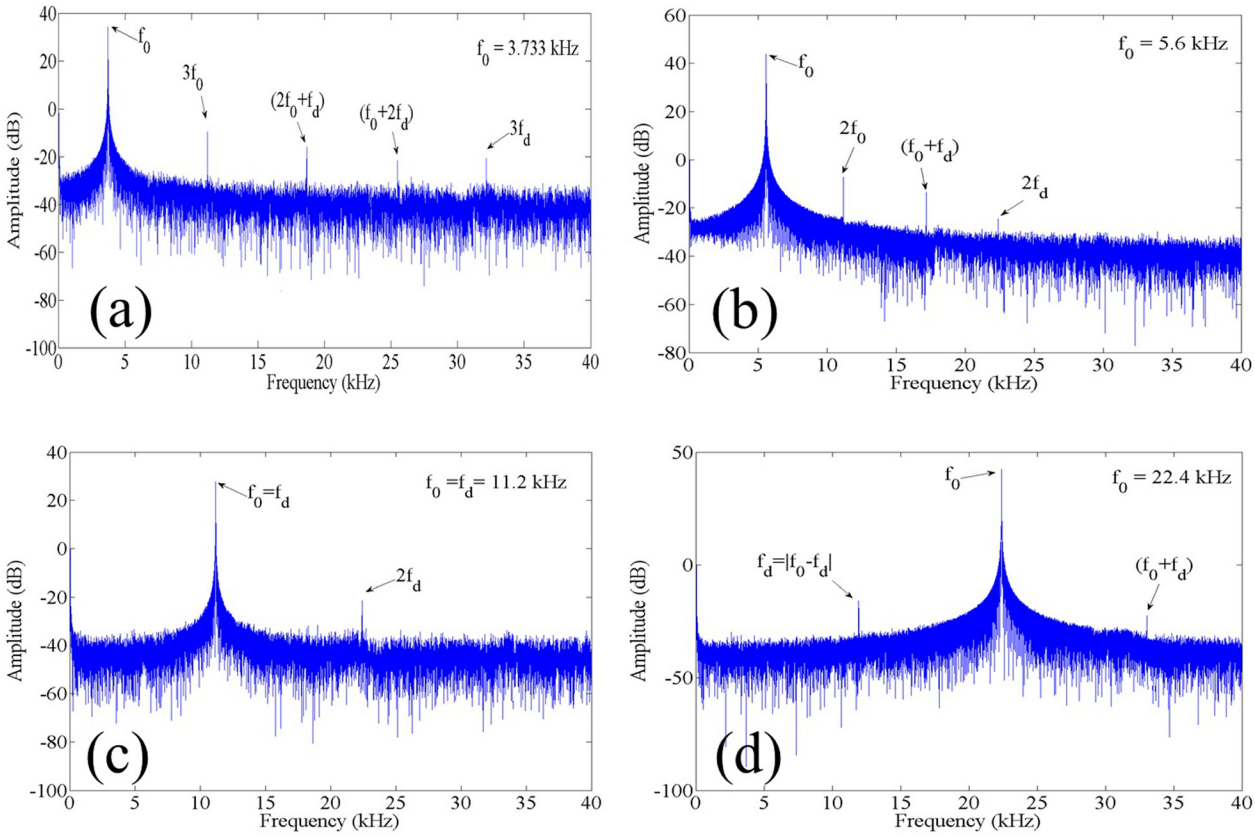

FIG. 6. (Color online) (a)–(c) Experimental nonlinear LDR effects measured at different input frequencies: 3.733 kHz (a), 5.6 kHz (b), 11.2 kHz (c), and 22.4 kHz (d). Each spectrum is measured at location (x_r, y_r) with the damage located at (x_d, y_d) and the transmitter at (x_t, y_t). The input voltage is 70 V.

periodic excitation to 5.6 kHz, similarly to the cubic approximation, also the nonlinear quadratic term allowed the generation of the nonlinear second order harmonic term $2f_0$, the superharmonic term $2f_d$ and the NDRI responses $|f_0 - f_d|$ and $(f_0 + f_d)$ [Fig. 4(b)]. Finally, the input frequency was changed to the second harmonic frequency range of the LDR (22.4 kHz). In this particular case the NDRI term $(f_0 - f_d)$ corresponded to the subharmonic resonance of the LDR [Fig. 4(c)]. However, the maximum vibration amplitude (out-of-plane displacement) of the nonlinear LDR over the entire structure is achieved at the damage location [see the linear solution (18)]. This is analytically illustrated in Fig. 5, which shows both linear and nonlinear flexural vibrations patterns on the composite laminate for the three different input frequencies.

From Figs. 5(a)–5(c), it can be seen that the nonlinear vibration pattern at $f_0 = f_d/3$, due to the cubic approximation, is able to reveal a local strong enhancement of the transverse nonlinear displacement at the damage location. Similar considerations can be made for the quadratic approximation associated to the frequencies $f_0 = f_d/2$ and $f_0 = 2f_d$ [Figs. 5(c) and 5(d) and 5(e) and 5(f)].

V. EXPERIMENTAL VALIDATION

Fully contact experimental tests were also carried out to validate the results of the theoretical model. The nonlinear structural responses were measured by the surface bonded PZT receiver sensor and the acquired signals for the above mentioned excitation frequencies (including the case of $f_0 = f_d$) at the input voltage of 70 V are reported in Fig. 6. This voltage value was chosen as the minimum one for the generation of "classical" and "non-classical" nonlinear elastic phenomena with different driving frequencies. Indeed, as it can be seen in Fig. 6, higher harmonics, superharmonics, and NDRI effects are clearly visible in the measured signals spectrum. Such nonlinear frequencies can be attributed either to the "clapping" motion of the region normal to the damage interface or to the nonlinear friction between the delamination surfaces, which are excited by small tangential stresses produced by the elastic waves propagating through the medium.

Therefore, the theoretical model here developed was able to predict the generation of nonlinear elastic effects, including NDRI, in the steady-state nonlinear LDR response. The experimental tests confirmed these predictions and showed that using continuous periodic excitation, the nonlinear structural phenomena could be also featured at locations different from the damage resonance. These results would provide opportunities for fully contact early detection and imaging of structural flaws. In addition, unlike standard nonlinear wave mixing and vibro-modulation techniques,[23] NDRI requires a single input frequency, which allows reducing electronic complexity for the disclosure of the nonlinear signatures.

VI. CONCLUSIONS

This paper aimed at developing a 2D theoretical model able to predict the generation of nonlinear elastic effects associated to the interaction of ultrasonic waves with the steady-state nonlinear response of LDR. LDR is used in nonlinear

elastic wave spectroscopy to enhance the excitation of the material damage at its local resonance. However, non-contact ultrasonic experiments have shown that, using wide-band excitation, the nonlinear damage response of the medium is confined exclusively at the defect location. The main result of this work was to prove both analytically and experimentally the generation of novel nonlinear elastic wave phenomena, here named as nonlinear damage resonance intermodulation, which correspond to a nonlinear intermodulation between the driving frequency and the defect resonance one. Beside these effects, also other nonlinear elastic wave phenomena such as higher harmonics and superharmonics were found. Transducer-based contact tests on a damaged composite laminate confirmed and validated these predictions and showed that using continuous periodic excitation, the nonlinear structural phenomena associated to LDR could be also featured at locations different from the damage resonance. These results can be used for multi-layered media and will provide opportunities for fully contact early detection and imaging of structural flaws.

ACKNOWLEDGMENTS

F.C. and M.M. acknowledge the EPSRC "NUSIT" (EP/N016386/1) and the EU FP-7 "ALAMSA" and Horizon 2020 "EXTREME" projects.

APPENDIX

In order to solve Eq. (23), we seek for a solution $Y^{p}_{mn}(t)$ of the form

$$Y^{p}_{mn}(t) = Y^{p1}_{mn}(t) + Y^{p2}_{mn}(t) = r(t)y_1(t) + s(t)y_2(t), \quad \text{(A1)}$$

where $r(t)$ and $s(t)$ are unknown functions. As Eq. (A1) should satisfy Eq. (23), first we find

$$Y'^{p}_{mn}(t) = r'(t)y_1(t) + s'(t)y_2(t) + r(t)y'_1(t) + s(t)y'_2(t). \quad \text{(A2)}$$

And assuming that $r(t)$ and $s(t)$ satisfy the following equation:

$$r'(t)y_1(t) + s'(t)y_2(t) = 0 \quad \text{(A3)}$$

we obtain

$$Y''^{p}_{mn}(t) = r'(t)y'_1(t) + s'(t)y'_2(t) + r(t)y''_1(t) + s(t)y''_2(t). \quad \text{(A4)}$$

Substituting Eqs. (A4), (A2), and (A1) into Eq. (23) and considering that y_1 and y_2 are the solutions of the homogenous part, we obtain

$$r'(t)y'_1(t) + s'(t)y'_2(t) = -\bar{F}^{II}_{mn}. \quad \text{(A5)}$$

Solving the systems of equations (A5) and (A3) for the unknown functions $r(t)$ and $s(t)$ yields

$$r(t) = \int_t \frac{y_2(\tau)\bar{F}^{II}_{mn}}{y_1(\tau)y'_2(\tau) - y_2(\tau)y'_1(\tau)}d\tau,$$
$$s(t) = -\int_t \frac{y_1(\tau)\bar{F}^{II}_{mn}}{y_1(\tau)y'_2(\tau) - y_2(\tau)y'_1(\tau)}d\tau. \quad \text{(A6)}$$

Substituting Eq. (A6) into Eq. (A1) with the use of Eq. (19) yields

$$Y^{p1}_{mn}(t) = \frac{\bar{A}^{II}e^{i2\pi f_{mn}t}}{4i\pi f_{mn}}\int_t e^{-i2\pi f_{mn}\tau}[\cos(2\pi f_0\tau) - \cos(2\pi f_d\tau)]^2 d\tau, \quad \text{(A7a)}$$

$$Y^{p2}_{mn}(t) = -\frac{\bar{A}^{II}e^{-i2\pi f_{mn}t}}{4i\pi f_{mn}} \times \int_t e^{i2\pi f_{mn}\tau}[\cos(2\pi f_0\tau) - \cos(2\pi f_d\tau)]^2 d\tau. \quad \text{(A7b)}$$

Therefore, assuming the displacement and velocity are equal to zero for $t=0$, the final solution of the problem (23) becomes

$$Y_{mn}(t) = \bar{A}^{II}\left[\frac{1-\cos(2\pi f_{mn}t)}{4\pi^2 f^2_{mn}} + \frac{\cos(2\pi f_{mn}t) - \cos(4\pi f_0 t)}{4\pi^2(4f_0^2 - f^2_{mn})} + \frac{\cos(2\pi f_{mn}t) - \cos(4\pi f_d t)}{4\pi^2(4f_d^2 - f^2_{mn})} + \frac{\cos[2\pi(f_0 \pm f_d)t] - \cos(2\pi f_{mn}t)}{\left[(2\pi f_0 \pm 2\pi f_d)^2 - 4\pi^2 f^2_{mn}\right]}\right]. \quad \text{(A8)}$$

The same analytical approach can be used to solve the third order problem [Eq. (30)].

[1]W. J. N. de Lima and M.-F. Hamilton, "Finite-amplitude waves in isotropic elastic plates," J. Sound Vib. **265**, 819 (2003).
[2]D. Broda, W. J. Staszewski, A. Martowicz, T. Uhl, and V. V. Silberschmidt, "Modelling of nonlinear crack–wave interactions for damage detection based on ultrasound—A review," J. Sound Vib. **333**(4), 1097–1118 (2014).
[3]M. Meo, U. Polimeno, and G. Zumpano, "Detecting damage in composite material using nonlinear elastic wave spectroscopy methods," Appl. Compos. Mater. **15**, 115–126 (2008).
[4]M. Scalerandi, A. S. Gliozzi, C. L. E. Bruno, D. Masera, and P. Bocca, "A scaling method to enhance detection of a nonlinear elastic response," Appl. Phys. Lett. **92**(10), 101912 (2008).

[5]F. Ciampa and M. Meo, "Nonlinear elastic imaging using reciprocal time reversal and third order symmetry analysis," J. Acoust. Soc. Am. **131**, 4316–4323 (2012).
[6]F. Ciampa and M. Meo, "Nonlinear imaging method using second order phase symmetry analysis and inverse filtering," J. Nondestruct. Eval. **34**(2), 7 (2015).
[7]F. Ciampa, G. Scarselli, S. Pickering, and M. Meo, "Nonlinear elastic wave tomography for the imaging of corrosion damage," Ultrasonics **62**, 147–155 (2015).
[8]A. Zagrai, D. Donskoy, A. Chudnovsky, and E. Golovin, "Micro- and macroscale damage detection using the nonlinear acoustic vibro-modulation technique," Res. Nondestruct. Eval. **19**, 104–128 (2008).
[9]F. Ciampa, S. Pickering, G. Scarselli, and M. Meo, "Nonlinear imaging of damage in composite structures using sparse ultrasonic sensor arrays," Struct. Control Health Monitor., 2016.
[10]M. Meo and G. Zumpano. "Nonlinear elastic wave spectroscopy identification of impact damage on sandwich plate," Compos. Struct. **71**, 469–474 (2005).
[11]L. D. Landau and E. M. Lifshitz, *Theory of Elasticity* (Pergamon, Oxford, 1986), Chap. III.
[12]S. Hirsekorn and P. P. Delsanto, "On the universality of nonclassical nonlinear phenomena and their classification," Appl. Phys. Lett. **84**, 1413–1415 (2004).
[13]R. A. Guyer, K. R. McCall, and G. N. Boitnott, "Hysteresis, discrete memory and nonlinear wave propagation in rock: A new paradigm," Phys. Rev. Lett. **74**, 3491–3494 (1994).
[14]I. Solodov, J. Bai, S. Bekgulyan, and G. Busse, "A local defect resonance to enhance acoustic wave-defect interaction in ultrasonic nondestructive evaluation," Appl. Phys. Lett. **99**, 211911 (2011).
[15]P. Johnson and A. Sutin, "Slow Dynamics and anomalous nonlinear fast dynamics in diverse solids," J. Acoust. Soc. Am. **117**, 124–130 (2005).
[16]G. De Angelis, M. Meo, D. P. Almond, S. G. Pickering, and S. L. Angioni, "A new technique to detect defect size and depth in composite structures using digital shearography and unconstrained optimization," NDT&E Int. **45**, 91–96 (2012).
[17]I. Solodov, J. Bai, and G. Busse, "Resonant ultrasound spectroscopy of defects: Case study of flat-bottomed holes," J. Appl. Phys. **113**, 223512 (2013).
[18]J. N. Reddy and C. M. Wang, "Relationship between classical and shear deformation theories of axisymmetric bending of circular plates," AIAA J. **35**(12), 1862–1868 (1997).
[19]I. Solodov, "Resonant acoustic nonlinearity of defects for highly-efficient nonlinear," J. Nondestruct. Eval. **33**, 252–262 (2014).
[20]J. N. Reddy, *Mechanics of Laminated Composite Plates: Theory and Analysis* (CRC Press, Boca Raton, FL, 1997).
[21]A.-C. Okafor, K. Chandrashekhara, and Y.-P. Jiang, "Delamination prediction in composite beams with built-in piezoelectric devices using modal analysis and neural network," Smart Mater. Struct. **5**, 338–347 (1996).
[22]I. Solodov, N. Krohn, and G. Busse, "Nonlinear ultrasonic NDT for early defect recognition and imaging," in *European Conf. on NDT (ECNDT)*, Moscow (June 2010).
[23]V. Zaitsev, V. Gusev, and B. Castagnede, "Luxemburg-Gorky effect retooled for elastic waves: A mechanism and experimental evidence," Phys. Rev. Lett. **89**, 105502 (2002).